InSense3D: Designing Smart 3D-Printed Structures Leveraging Ferromagnetic Filaments for Inductive Deformation Sensing

Rahul Bhaumik
Faculty of Engineering
Free Universitv of Bozen-Bolzano
Bolzano, Italy
Human Computer Interaction Institute
Carnegie Mellon University
Pittsburgh, Pennsylvania, USA
rbhaumik@unibz.it

Camilo Ayala-Garcia
Faculty of Design and Art
Free University of Bozen-Bolzano
Bolzano, Italy
camilo.ayalagarcia@unibz.it

Niko Münzenrieder
Faculty of Engineering
Free University of Bozen-Bolzano
Bolzano, Italy
niko.muenzenrieder@unibz.it

Michael Haller
Faculty of Engineering
Free University of Bozen-Bolzano
Bolzano, Italy
michael.haller@unibz.it

Alexandra Ion
Human Computer Interaction Institute
Carnegie Mellon University
Pittsburgh, Pennsylvania, USA
alexandraion@cmu.edu

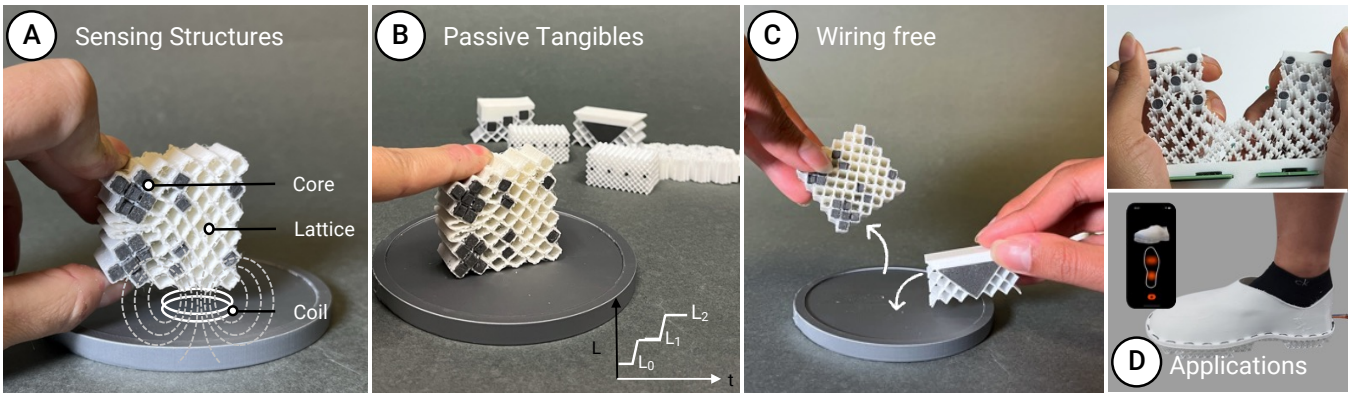

Figure 1: Our proposed sensor comprises ferromagnetic components (cores) within deformable 3D-printed lattice structures, arranged in proximity to a readout coil generating a magnetic field (A). Examples of structures produced through different configurations of ferromagnetic cores and lattice substrates are shown, each tailored for specific use-case scenarios. These configurations distinctively influence the underneath coil's inductance when any external force is applied (B). A key characteristic of such passive tangibles is that they can be integrated with the coil in a wireless manner and can easily be swapped across the coil surface depending upon user's needs without requiring any complex assembly with the electronic components (C). Example applications to showcase the sensor's functioning include a stretchable handheld controller and a smart pressure-sensitive shoe sole with embedded ferromagnetic particles, which is able to detect the deformation when external pressure is applied (D).

Abstract

In this paper, we explore the design and development of *passive* soft 3D-printed structures whose deformation can be sensed accurately without any wired connection. By 3D printing tangible interfaces consisting of flexible TPU (thermoplastic polyurethane), made from lattice structures with bespoke geometries and mechanical properties, and ferromagnetic elements using metal-infused filaments, we enable the detection of structural deformations through inductive sensing. We investigate how different ferromagnetic core configurations within flexible substrates, guided by key design parameters, influence the sensitivity, responsiveness, and deformability of the sensing system. We demonstrate that our 3D-printed inductive sensing approach allows users to switch their fully passive tangible interfaces for specialized tasks without assembly or the need to unplug wires. Our sensing approach can be integrated in portable

CHI '26, Barcelona, Spain

ACM ISBN 979-8-4007-2278-3/26/04
https://doi.org/10.1145/3772318.3791824

applications, such as a smart bottle cover that captures subtle deformation to measure liquid intake, or in wearable applications, such as monitoring foot pressure in smart shoes.

CCS Concepts

• Human-centered computing → Human computer interaction (HCI); **• Computer systems organization → Sensors and actuators**.

Keywords

Inductive Sensing, 3D Printing, Deformable Sensor, Ferromagnetic Parts, Flexible Lattice

ACM Reference Format:

Rahul Bhaumik, Camilo Ayala-Garcia, Niko Münzenrieder, Michael Haller, and Alexandra Ion. 2026. InSense3D: Designing Smart 3D-Printed Structures Leveraging Ferromagnetic Filaments for Inductive Deformation Sensing. In *Proceedings of the 2026 CHI Conference on Human Factors in Computing Systems (CHI '26), April 13–17, 2026, Barcelona, Spain.* ACM, New York, NY, USA, 17 pages. https://doi.org/10.1145/3772318.3791824

1 Introduction

People increasingly expect everyday objects to respond to touch, pressure, and motion. Such rich tangible interactions can blur the boundary between the physical world and digital systems. To date, sensing approaches have been used to recognize hand grips on doorknobs [25], to turn walls into touch surfaces [28], or to enable interactive paper toys and pop-up books [17]. In other words, these examples demonstrate the promise of augmenting what we already have.

Beyond augmenting existing objects, personal fabrication gives designers freedom to create tangible interfaces, custom-shaped to fit specific tasks, or conditions. 3D printing, in particular, allows functional geometries to be designed with integrated sensing elements using conductive filaments. This enables custom form factors and interaction affordances, such as free-form objects with touch sensing [26], or soft bodies with integrated deformation sensing [8, 24], that can be printed in one go. Most interactive 3D printed objects utilize capacitive or resistive sensing, which often come with practical drawbacks: hysteresis limits accuracy and drift requires frequent recalibration.

Inductive sensing is a compelling alternative. Widely used in engineering for displacement and strain, inductive methods offer high sensitivity, low hysteresis, and stable, continuous measurements [3, 14, 20]. Recent HCI work has begun to leverage such inductive mechanisms for deformation sensing by embedding coiled metal wire in 3D-printed shapes [15]. However, all sensing approaches in 3D-printed interfaces, whether capacitive, resistive, or inductive, require post-print assembly of electronic components, which can become very cumbersome.

In this paper, we introduce *InSense3D*, a sensing approach that preserves the benefits of inductive sensing while eliminating the need to wire the tangible itself to any readout, thereby eliminating assembly of any electronics all together, cf. Figure 1. The printed *tangible is fully passive*. It consists of a *deformable lattice* with carefully arranged *ferromagnetic cores*. During interaction (e.g., push, squeeze, shear), the lattice deforms and the cores move relative to the stationary coil that is close to it, modulating the coil's inductance. The electronics measure this inductance change to infer the deformation state. The key advantage is that the coupling is contactless, so the tangible requires no wires, connectors, or onboard components: users can switch interfaces simply by placing another passive print onto the same sensing pad (e.g., flush-mounted in a desk or embedded in a portable object base), without the need to unplug or reconnect cables. Our approach provides ease for users (as they can update their tangible by simply 3D printing their new passive structure), while preserving the high-quality sensing data of inductive sensing (i.e., high-sensitivity readings with low hysteresis, low drift, and sustained, continuous sensing). Finally, we demonstrate how core placement, core geometry, and lattice stiffness can be tuned to shape response curves, separate normal and shear axes, and modulate sensitivity across the surface.

In summary, this paper makes the following *contributions*:

(1) **A wiring-free inductive sensing principle for 3D-printed tangibles**, in which a passive, deformable lattice with embedded ferromagnetic cores is read by a stationary flat coil and electronics.
(2) **A design space and guidelines** covering core configurations, lattice parameters, and coil–core coupling that yield one- and multi-axis deformation sensing with tunable sensitivity and low hysteresis.
(3) **Technical validation** comparing inductive response and stability against other representative 3D-printed sensing approaches, highlighting reduced calibration burden and improved repeatability.
(4) **Application examples** that leverage this exchangeability of interfaces - e.g., pressure-sensitive lattice for liquid volume measurement, on-surface controllers, and so on - each of which can be replaced on the same embedded coil without reconnecting wires.

Taken together, our approach enables custom, high-fidelity tangible interfaces that are as easy to swap as they are to print, lowering the barrier to iterative design while maintaining the sensing performance needed for rich user experiences.

2 Related Work

Prior to our exploration of pressure-sensitive 3D-printed structures, we reviewed existing research that leverages additive manufacturing to enable complex, deformable geometries and integrates sensing capabilities — ranging from resistive and capacitive methods to inductive sensing — within printed structures.

2.1 3D Printing for Complex, Deformable Structures

3D printing techniques, especially fused deposition modeling (FDM), have enabled the fabrication of intricate geometries and flexible structures that exhibit controlled or pre-specified deformation behavior. For instance, Ion et al. [12, 13] demonstrated the concept of metamaterial mechanisms, which comprise combinations of different types of cells within a monolithic structure that act together in a systematic way to produce macroscopic movement. Thus, by combining rigid cells with shearing or deformable cells, various functional mechanisms — such as door latches or pliers — can

be realized within a single 3D-printed structure, eliminating the need for any post-print assembly. Studies have also explored lattice structures with open- and closed-cell topologies — such as body-centered cubic (BCC), face-centered cubic (FCC), Schwarz, etc. — and with varying cell sizes, to evaluate their mechanical behavior under deformation, with all structures fabricated through FDM printing using thermoplastic polyurethane (TPU) filament [4]. In addition to FDM, selective laser sintering (SLS) using TPU powder has also been utilised to fabricate and evaluate soft lattices with different beam radii and relative densities, for large deformations [10]. Similarly, in our study, based on specific use cases and sample testing, we have utilized FDM-manufactured square-celled grid structures and beam-based unit cell geometries — which allow for both deformation and the integration of rigid core elements — to fabricate the substrate in our sensing structures.

2.2 Deformable Materials and Sensing

Deformable materials, such as mechanically reconfigurable metamaterial structures, have been increasingly utilized to integrate sensing capabilities by taking advantage of changes in their structural configuration under external forces or relative displacement between their internal parts. For instance, metamaterial structures have been utilized to tune electromagnetic resonance by physically deforming the printed geometry through stretching, compression, or bending [1]. Similarly, soft mechanical metamaterials incorporating silver–TPU conductive networks have been designed to perform digital logic operations, wherein the conductive pathways open or close in response to mechanical deformation [7]. Likewise, region-specific deformation sensing can also be enabled by embedding conductive channels within bendable compliant structures, where the deformation is detected by identifying which circuit pathways remain closed or open [18]. Leveraging internal movable parts in a structure, functional capacitive accelerometers have been fabricated using multimaterial printing [19]. Furthermore, coil geometries have been incorporated in deformable materials like textiles for contact-based sensing on surface using textile-specific processes like embroidery [9]. In our case, we utilize the soft recoverable structures with moving internal parts for inductive-based deformation sensing. In all of the aforementioned works, various fabrication processes have been employed ranging from 3d-printing of molds, multimaterial printing, laser cutting, embroidery and so on; however we focus on primarily FDM-based 3d-printing for the ease of fabrication processes so that they can even be utilized by novice users.

2.3 3D-Printed Structures with Integrated Sensing

Building upon structural complexity, several studies have demonstrated the integration of sensing capabilities into 3D-printed structures, primarily utilizing capacitive or resistive sensing to detect deformations, displacement or any applied forces. For instance, MetaSense [8] presents a method to integrate sensing capabilities into 3D-printed mechanical metamaterials. It does this by incorporating conductive shear cells, which function as capacitive sensors that detect deformation through capacitance changes. The study indicates that even small cells (5 mm) can reliably sense deformation, though larger cells provide better signal-to-noise ratios. Moreover, studies have been conducted to fabricate smart structures through fused deposition modeling-based multimaterial 3D printing, wherein filaments with both flexible and conductive properties have been developed (by combining carbon black with TPU) and used alongside other filaments (e.g., pure TPU) [23]. Additionally, Sakura et al. [24] propose lattice-based FDM-printed soft sensors using conductive and non-conductive filaments, wherein changes in resistance are recorded when the sensor structure is deformed. The study lays the parameters for lattice design to alter the flexibility and nature of deformation, such as compression, shear, or twisting in the sensing structure, which became a guiding factor in designing certain flexible substrate geometries in our proposed sensors. In contrast to these approaches, our method eliminates the need for additional cabling within the 3D prints by suspending the ferromagnetic core in the vicinity of an external sensing coil. However, we leverage multimaterial printing techniques to integrate ferromagnetic-PLA elements into TPU-based flexible substrates for inductive sensing. In a slightly different approach, Truby et al. [27] propose a fluidic innervation technique that enables self-sensing capabilities within 3D-printed structures using a single build material, where deformation is detected through pressure changes in embedded fluidic channels. Additionally, in another study - eFlesh [21], a low-cost, 3D-printable magnetic tactile sensor that combines microstructured TPU lattices with embedded magnets and Hall-effect sensing is showcased to capture fine-grained deformations. However, in our approach we leverage custom printing of ferromagnetic parts in different shapes and sizes (ranging from a solid prism-shaped insert to multiple distributed elements embedded within lattice-cell pockets) for distinct use cases (such as controllers or load-measurement scenarios, as discussed later in section 8) instead of using commercially available magnets.

2.4 Inductive Sensing in 3D-Printed Geometries

While resistive and capacitive methods are quite prevalent, inductive sensing is emerging as a promising approach for capturing deformation in 3D-printed structures or flexible substrates. For instance, Lee and He [15] demonstrate a novel approach using a helix-and-lattice structure within a 3D geometry to detect deformations in the object, such as bending, twisting, and compression, through inductive sensing. This approach utilizes the insertion of steel wire in the embedded hollow helical channels to measure the change in inductance when current is passed through the wire, and the wire deforms due to an external force. In contrast, we keep the geometry of the coiled wire constant and fixed in space and solely alter the magnetic field around the coil using controlled displacement of the ferromagnetic parts in the vicinity. Lee et al. also present a tool that converts an input 3D object into a customized and printable wireframe, lattice, and helical structure so that the structure exhibits desired sensing properties [16]. Similarly, in a study by Babkovic et al., a double-spiral-shaped inductive sensor composed of polylactic acid (PLA) filament with embedded conductive wire has been demonstrated [2]. The designed structure is deemed useful for measuring force or displacement through changes in self-inductance. An alternate approach to inductive sensing in soft

substrates involves adding ferromagnetic particles within elastomer matrices, enabling high sensitivity and the capability to measure physiological parameters like arterial pulsations [14, 20]. Studies have also further investigated the effects of iron powder fillers with varying particle sizes in bio-compatible silicone elastomers with regard to the sensor's sensitivity [22]. Unlike earlier approaches that relied on embedding conductive wires into deformable lattice or using ferromagnetic silicone composites, our method extends the scope of inductive sensing. It is inspired by the work of Bhaumik et al. [3], who demonstrated how embedding ferromagnetic elements into a soft, 3D-printed lattice of varying stiffness enabled sensing based on core–coil separation. However, in this study, we extend beyond core–coil separation as the sole factor for sensing deformation by examining additional geometric and spatial factors of the ferromagnetic core, such as offset, density, and size, along with their different combinations to enable customized sensor designs. Moreover, by leveraging variable sensitivity across different regions through a single readout coil to enable spatially resolved deformation detection, and by employing diverse lattice configurations for stretchability and multi-axis deformation, our approach remains distinct from prior work.

3 InSense3D - Our Approach

Our approach builds on the principle of inductive sensing [6]. As illustrated in Figure 2, introducing a ferromagnetic material near a coil alters the local magnetic permeability, concentrating the flux in that region.

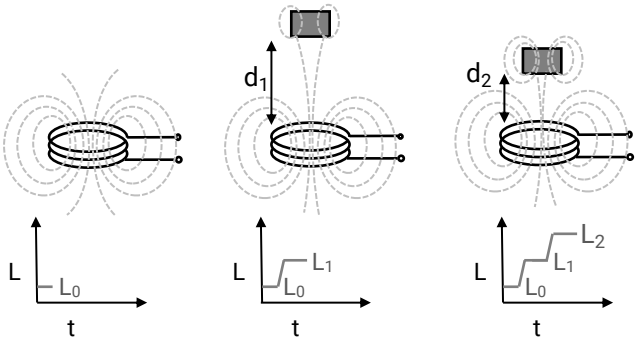

Figure 2: Our proposed approach primarily based on the principle of change in inductance due to the change in relative position of a ferromagnetic material near a coil. No Ferromagnetic material near the coil (left); Ferromagnetic material introduced near the coil at distance d1 (middle); Ferromagnetic material brought more closer at distance d2 from coil where d2 < d1 (right).

This flux change modifies the coil's inductance. Moving the ferromagnetic material closer to the coil (where the magnetic field is stronger) increases its influence and further raises the inductance, up to the point where the magnetic core is fully inserted into the coil. Thus, different positions of the ferromagnetic material relative to the coil lead to varying magnetic field interactions and, consequently, distinct inductance values, as shown in Figure 2.

3.1 Control Core Placement

Building on the principle that inductance depends on the separation between core and coil, we design our sensor structure by positioning the ferromagnetic core at a distance of roughly one core diameter or less from the coil, using a support medium, the lattice. The lattice not only secures the core material close to the coil, but also plays a decisive role in defining and stabilizing the core–coil spacing (cf. Figure 3).

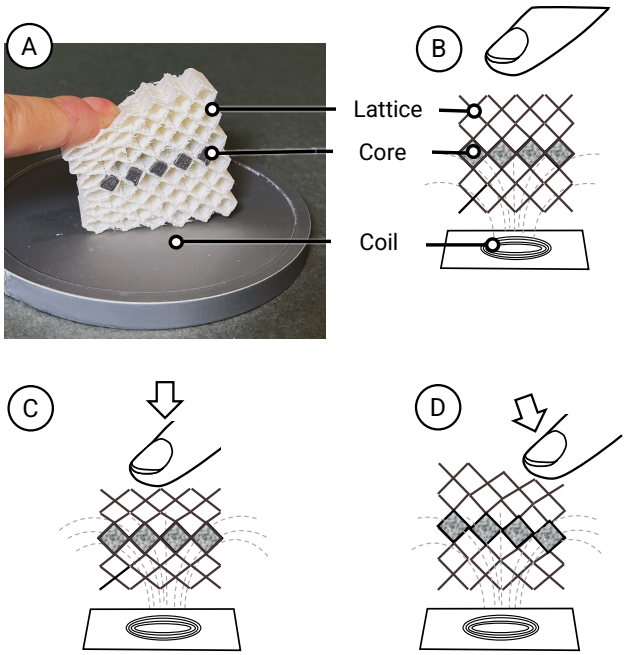

Figure 3: Our sensing approach comprising the ferromagnetic core elements embedded within a deformable lattice placed above the readout sensing coil (A). The system in its natural, unpressed state (B); Homogeneous pressing of the lattice at the center of the interface (C); localized pressing of the lattice, leading to non-uniform geometry deformation (D).

A key requirement of our approach is that this lattice structure must be both deformable and elastic, enabling it to respond to external forces while recovering its original shape once the load is removed. To achieve this, we integrate repeating cellular or beam-based lattice geometries — such as a Body-Centered Cubic (BCC) unit cell — into the design, making the structure porous and compressible (cf. Figure 3). These lattices are manufactured through fused deposition modeling (FDM) using soft materials like Thermoplastic Polyurethane (TPU), which allows fine-tuning of the mechanical properties, particularly elasticity. When an external force deforms the lattice, the suspended core shifts accordingly, altering its distance from the coil and thus changing the inductance. From a fabrication perspective, a major advantage of this approach is that both the flexible lattice and the ferromagnetic core can be 3D-printed. This enables the creation of custom geometries for diverse application scenarios, with the core being produced using a ferromagnetic PLA composite.

3.2 Wire-free Integration

A key advantage of our approach is the wire-free integration: the 3D-printed lattice can be directly placed onto a readout coil without requiring any internal electrical connections to the readout circuitry. The lattice–core interface remains fully passive and is merely positioned on top of, or near, the active coil system, which houses the inductance-to-digital converter (LDC) and the microcontroller (cf. Figure 4).

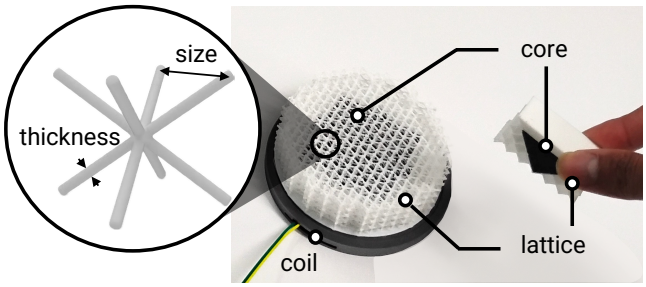

Figure 4: Both key components — the lattice (with its unit cell, shown in left) and the core — are entirely passive and require no additional cabling, enabling a wire-free readout between the different sensor interfaces and the generic coil system embedded in the substrate base.

No additional physical wiring is required between the structure and the electronic components, which greatly simplifies both fabrication and assembly. From a design perspective, this separation enables the readout electronics to remain entirely outside the deformable interface, enhancing robustness, modularity, and recyclability while reducing unnecessary electronic waste. It hence opens up the possibility of creating soft, durable, and electronically decoupled interactive surfaces. This configuration supports modular design flexibility, where different substrate-core assemblies can be easily swapped or repositioned over the same coil surface to accommodate varied use cases or interaction scenarios. The versatility in how the lattice structure and embedded core are structured enables different displacement behaviors of the core, leading to distinct inductance patterns — all while using the same underlying electronics. Ultimately, the absence of internal wiring between the substrate and the sensing system enables easy disassembly and reconfiguration, supporting a wide range of sensing and interaction applications with minimal hardware complexity.

3.3 High Sensitivity

Finally, one of the key characteristics of our approach is its high sensitivity, particularly when the ferromagnetic core is positioned closer to the coil, resulting in stronger magnetic coupling. In such a state, even slight displacements of the core can lead to measurable changes in the coil's inductance. This enables the sensing coil to detect subtle variations in structural deformation, even due to a small loads which causes a distinct change in the inductive response, highlighting the system's sensitivity to low-pressure inputs. In *InSense3D*, we are able to detect fine-grained displacements of the core, made possible by the use of soft, deformable lattice-based structures. These subtle shifts result in measurable changes in inductance, highlighting the high sensitivity of the system and making our approach well-suited for real-world applications.

4 Design Parameters and Evaluation

Related work shows that multiple factors within the inductive sensing system influence the performance of the inductive signal [20]. For instance, prior studies have shown that external pressure deforming the geometry of the sensing coil change the measured inductance [22]. In this paper, we use a rigid, non-flexible coil while various factors can affect the magnetic permeability in its vicinity. Specifically, we systematically position ferromagnetic components near the coil to alter the inductive response of the coil. In the following sections, we present the key design parameters that govern the inductance response in different core–coil configurations and evaluate how each factor individually contributes to the overall sensing behavior.

4.1 Design parameters affecting sensing

We note that, apart from the distance between the ferromagnetic core and the coil, different geometric configurations of the core (e.g., size, shape, density etc.) influence the coil's inductance, providing richer design opportunities for developers of such interactive tangibles. In the following, we have identified four fundamental key factors that shape the design direction of our soft inductive pressure sensors. They include *distance*, *offset*, *size*, and *density* of the core material inside the flexible lattice, as we illustrate in Figure 5 and detail in the following.

Distance: The distance d between the core and the coil plane (cf. Figure 5) directly determines pressure sensing. When external forces push on the flexible structure, this distance changes, shifting the coil's inductance as the core moves closer and increase the coil´s inductance.

Offset: The offset o describes how far the core is shifted sideways from the coil's central axis, cf. Figure 5. A larger offset places the core asymmetrically near the coil, so the same pressure on different regions produces uneven inductance changes. This happens because anisotropic lattices, such as TPU-based BCC structures, deform differently depending on where the force is applied, displacing the core in a position-dependent way and creating specific inductance variations.

Size: The size s describes the dimension of the core, such as the edge length of its cross section, cf. Figure 5. A larger core means more ferromagnetic material near the coil, which increases local magnetic permeability and strongly affects the coil's total inductance.

Density: The density ρ describes how much ferromagnetic material is present per unit volume when multiple cores are embedded, cf. Figure 5. Evenly spaced cores define their average separation, but under compression they cluster together, raising magnetic permeability and boosting inductance similar to having a single larger core. When pressure is released, the particles spread out again, weakening magnetic coupling and reducing the inductance. As the amount of magnetic material introduced inside the lattice structure increases, the average separation between the core parts decreases, and

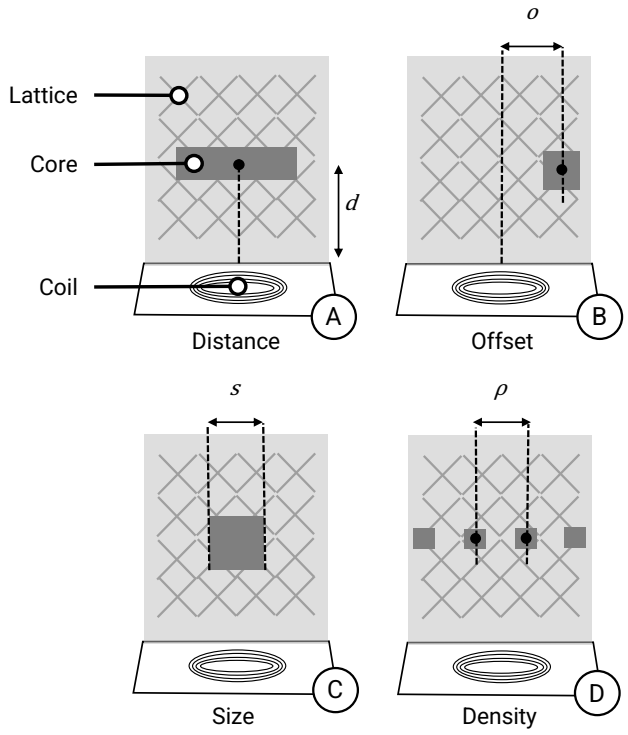

Figure 5: Fundamental design parameters of the ferromagnetic core material in our proposed sensing structures. Distance of the core from the readout coil (A), Lateral offset of the core from the vertical axis through the coil center (B), Size of the core as determined by the edge length of the core geometry (C), and inter-core separation signifying the core's distribution density within the substrate, for multi-piece core configurations (D).

vice-versa. Instead of calculating the absolute ferromagnetic mass to sensor volume ratio, here we consider the inter-core separation (or ρ) for designing and evaluating sensitive lattice structures with customizable core configurations.

Other factors, such as varying the infill density of 3D-printed ferromagnetic components, obviously also impact the inductance reading of the coil, as changing the infill density increases the effective permeability within the same core volume. However, this aspect is beyond the scope of the present study. Instead, for our samples, we used a single commercially available filament[1] with fixed ferromagnetic particle density and printed all parts at 100% infill to ensure consistency. This allowed us to focus solely on the effects of geometric and spatial core configurations without introducing material-level variation.

4.2 Evaluating Design Parameters

We then systematically evaluated how these four design parameters influence sensor sensitivity by analyzing the coil's inductance response. The goal of these experiments is to validate that various lattice-core combinations yield robust sensor readings, which supports replicability and enables readers to build on our work. To do this, we varied each parameter independently in sensor prototypes that combined flexible lattices with embedded ferromagnetic cores and a housing together with the readout electronics, cf. Figure 6.

The housing enclosed the lattice and the PCB coil and integrated three pushable tips, each capable of compressing the lattice by 10 mm. Pressing all tips applied a global compressive strain of about 25%, while pressing a single tip generated localized, non-uniform deformation. This setup enabled us to investigate both global and local effects. In certain configurations, we reinforced selected lattice cells to channel force transmission more directly towards the core.

For all experiments, we used the same planar PCB coil (Texas Instruments, 30 turns, four layers, Ø=29 mm), paired with a capacitor to form an LC resonant circuit and connected to an LDC1614 inductance-to-digital converter with an MSP430 microcontroller.

4.2.1 Distance. To get a deeper understanding of how the core-to-coil distance influences the sensitivity, we fabricated a 3D-lattice with the ferromagnetic layer embedded at four distances above the coil with d=11 mm ($\approx \frac{1}{3}\times$ coil diameter Ø), d=14.7 mm ($\frac{1}{2}\times$ coil diameter), d=29 mm (1× coil diameter), and d=42 mm (1.5× coil diameter). For each variant, we used the same flexible structure (44 mm × 20 mm × 44 mm, TPU NinjaFlex 85A, cell size 4.2 mm, wall thickness 0.8 mm) with compressible cellular geometry for repeatable deformation cycles. For the ferromagnetic cores, we used the Protopasta Magnetic Iron PLA. For every configuration, the core layer was compressed by 10 mm, (by applying an uniform load on the sensor top surface using our testing fixture) and the relative inductance change ($\Delta L/L_0$) was measured. Each compression step was repeated three times, and mean/variance values of inductance shift were computed for comparison.

4.2.2 Offset. We also studied the effect of lateral core displacement from the coil's central axis by embedding a 9 mm × 9 mm ferromagnetic core at three offsets: (1) centered (o=0 mm), (2) midway toward the edge (o=7.2 mm $\approx \frac{1}{4}$ coil diameter), and (3) at the coil edge (o=14.7 mm $\approx \frac{1}{2}$ coil diameter). For each offset, we applied a pointed load at three surface positions using the testing setup, compressing the lattice by 10 mm ($\sim$ 25% strain). The three load positions on the lattice top layer were located at 0 mm, 20 mm, and 40 mm, respectively, from the top-left corner. At each of these points, we applied the load locally by pressing one of the three movable tips of the housing. For every core-offset configuration, we recorded the corresponding change in coil inductance after applying the force at each point on the lattice. Again, we repeated each measurement three times and computed the mean and variance of the relative inductance change.

4.2.3 Size. We also tested three core sizes with surface areas of approximately 5 mm × 5 mm, 10 mm × 10 mm, and 15 mm × 15 mm, each with a depth of 20 mm. The vertical distance between the core center and the coil plane was kept constant at 20 mm, corresponding to about two-thirds of the coil diameter. We applied a uniform external pressure that displaced each core by 10 mm. For every core size, we carried out three compression tests and then

[1] https://proto-pasta.com/products/magnetic-iron-pla

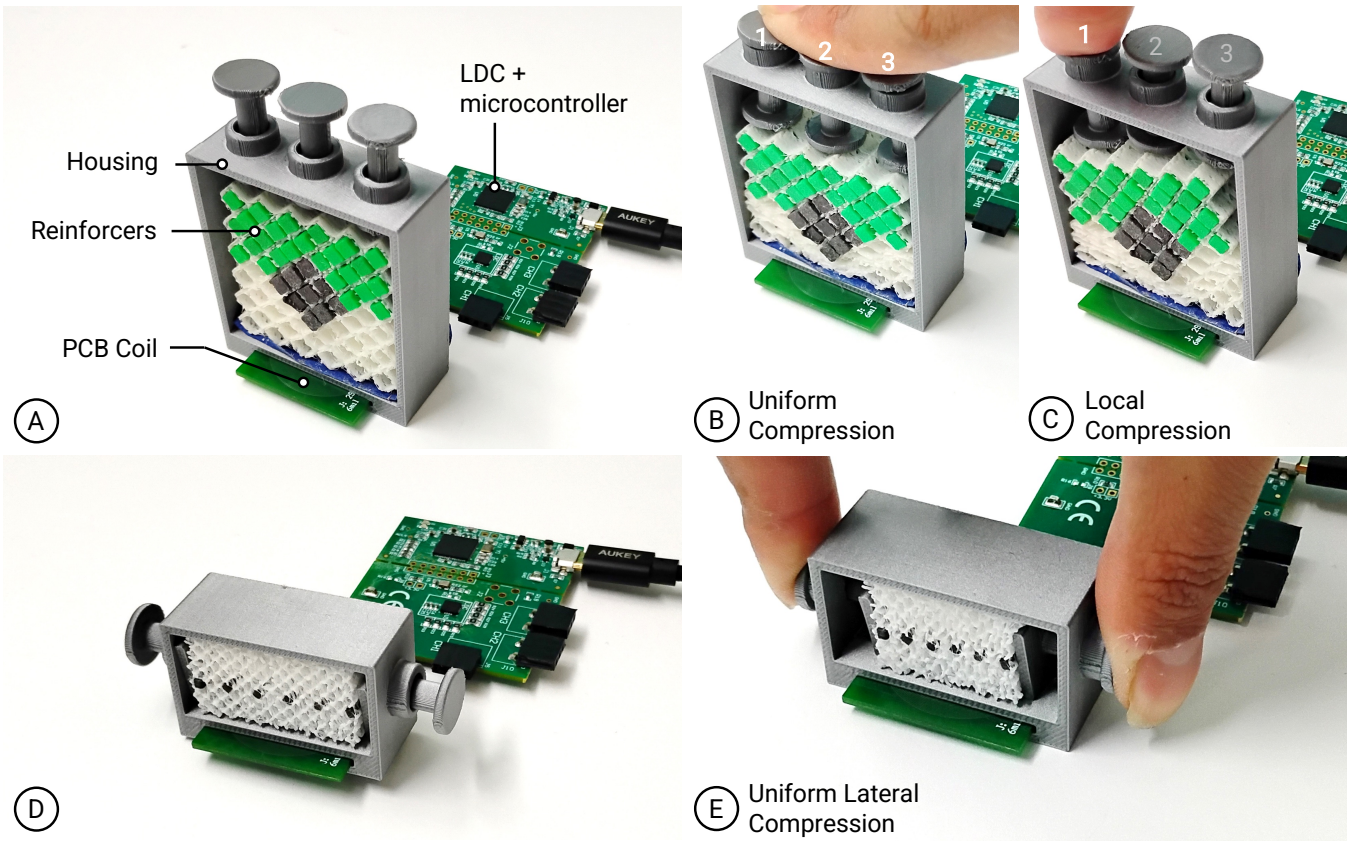

Figure 6: The experimental apparatus showcasing how the assembled sensor lattices are housed alongside the readout electronics comprising the planar PCB coil, LDC1614, and MSP430 microcontroller (A). The housing with pushable tips, which, when simultaneously pressed, creates a uniform compression in the lattice up to 25% strain, whereas the same housing can also provide localized compression at specific points along the sensor top-side (B, C). The testing setup used to apply uniform lateral compression onto the sensor structure (D), compressing a lattice till one-third of its initial width (E).

calculated the mean and variance of the relative inductance change for comparison.

4.2.4 Density. To investigate the effect of multi core density, we fabricated three lattice samples with different inter-core separations. A TPU lattice (2 mm unit cell size, 0.2 mm thickness) embedded ferromagnetic elements at core-to-lattice volume ratios of 1.1%, 2.2%, and 3.3%, corresponding to inter-core distances of 18 mm, 12 mm, and 7 mm, respectively. We aligned the coil parallel to the axis connecting the cores and applied horizontal compressive strain of up to 33% along this axis. During compression, we recorded the relative inductance change ($\Delta L/L_0$), repeating each test again three times.

We fabricated the samples by 3D-printing the TPU lattice and ferromagnetic cores separately and adding PLA reinforcers for stiffness, which allowed quick prototyping and testing. As an alternative, we can co-print the TPU lattice and ferromagnetic cores using dual-nozzle extrusion, eliminating the need for post-print assembly.

4.3 Results

Figure 7 provides an overview of the overall results and illustrates the influence of each parameter.

The relative inductance change decreases as the core-coil distance increases. At the smallest distance of 11 mm, the relative change was 0.70% ± 0.01, dropping to 0.39% ± 0.03 at 14.7 mm, 0.03% ± 0.001 at 29 mm, and just 0.01% ± 0.001 at 42 mm. The largest inductance shift thus occurs when the core is positioned closest to the coil.

Regarding the offset, at zero offset the response is symmetric: the inductance change peaks at the center (0.36%) and is nearly identical at both ends with about (0.13%–0.14%), cf. Figure 7. As the core moves away from the central axis, the inductance response becomes uneven across the surface. At half the coil radius offset, for example, the leftmost point shows the smallest change (0.03%), while the center and rightmost points remain equal at about (0.17%). At a full coil radius offset, the inductance change increases steadily from left to right, ranging from (0.003%) to (0.045%) and up to (0.077%).

As the core size (cross-sectional surface area) increases from 5 mm × 5 mm over 10 mm × 10 mm to 15 mm × 15 mm, the relative

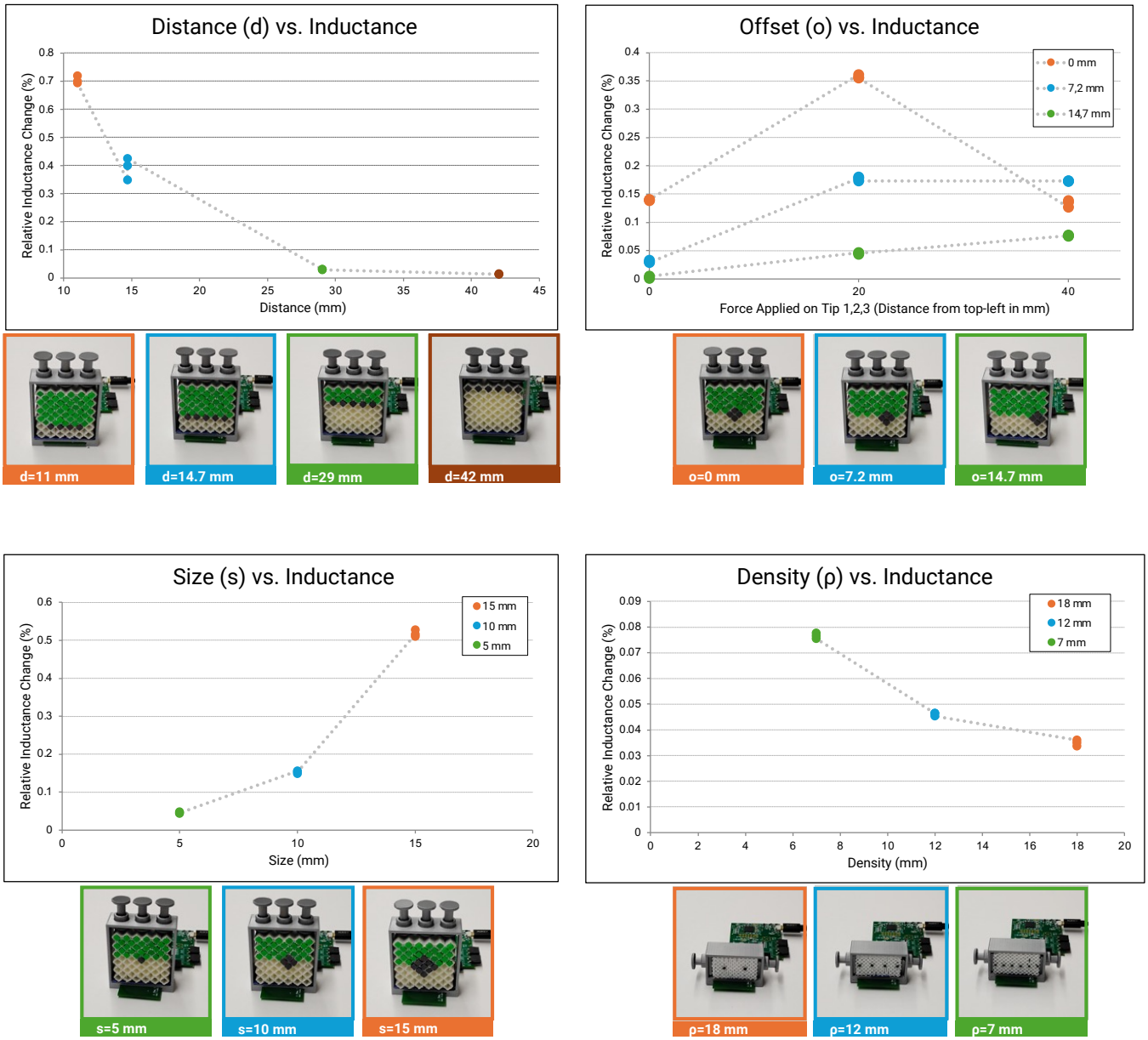

Figure 7: Plots showcasing the effect of each fundamental design parameters—distance, offset, size, and core density—on the relative inductance change (%) of the coil.

inductance change rises markedly. Here, the core-coil distance is the same (10 mm) in all cases, cf. Figure 7. For example, the relative inductance changes for core sizes of 5 mm, 10 mm, and 15 mm were (0.05% ± 0.001), (0.15% ± 0.03), and (0.52% ± 0.07), respectively. This increase is explained by the higher magnetic permeability introduced in a larger volume near the coil, which amplifies the inductance.

For an inter-core separation of 18 mm, the relative inductance change was (0.04% ± 0.001), rising slightly to (0.05% ± 0.001) at 12 mm and reaching (0.08% ± 0.001) at 7 mm. Smaller gaps between cores - meaning higher core densities - produce larger inductance changes under compression, since clustered multi-cores increase the magnetic permeability around the coil.

5 Combining multiple parameters

By combining the four design parameters, we can construct more complex core arrangements that capture richer motion patterns and enable customized interfaces. In this section, we explore, for example, scenarios where core–coil distance and offset act simultaneously, or where distance is paired with size, size with offset,

and distribution with either offset or size. These combinations can produce customized core shapes, including asymmetric configurations, which in turn strongly affect the overall inductance shift when external forces act on different regions of the substrate. The following subsections describe these configurations in detail.

5.1 Distance + Offset

As shown in Figure 8, we tested two implementations. In the single-piece core configuration, the core element is positioned at a 45° angle within the lattice, resulting in a continuously and linearly varying distance from the coil. In contrast, the multi-piece core configuration uses three separate core elements placed at descending heights of 36 mm, 28 mm, and 20 mm, with lateral offsets of −16 mm, 0 mm, and 16 mm from the coil axis, respectively, within the lattice.

To test the sensitivity of the structure, we applied a pointed load at three locations on the top of the cover, positioned at 0 mm, 20 mm, and 40 mm from the top-left edge. At each location, the lattice was compressed by about 10 mm (roughly 25% strain), and the resulting relative inductance change of the coil was recorded.

The measurements showed that the smallest inductance change occurred at the end with the largest separation, and the maximum change at the opposite end. For example, the three test locations yielded inductance changes of (0.04 ± 0.01), $(0.11 \pm 0.01\%)$, and $(0.18 \pm 0.02\%)$ in one setup, while in the other setup the values were $(0.02 \pm 0.003\%)$, $(0.03 \pm 0.002\%)$, and $(0.06 \pm 0.001\%)$, respectively, cf. Figure 8.

In the multi-core configuration, the dominant factor was the core-coil separation as the substrate is compressed. However, the offset also contributes: pressing on the leftmost region of an anisotropic lattice caused neighboring cores to shift, which in turn affected the overall inductance response.

5.2 Distance + Size

In this configuration, we used a single core piece where both the vertical distance between the core and the coil, as well as the effective core size, varied linearly along the substrate. At the left edge, the core had an effective edge length of about 5 mm with a core-coil separation of 38 mm, while at the right edge the edge length increased to about 35 mm with a core-coil gap of only 8 mm.

We evaluated the sensitivity by applying a pointed load at three locations along the top surface of the lattice and recorded the resulting inductance changes. The smallest shift occurred at the end where the core was farthest and thinnest $(0.04 \pm 0.01\%)$ at the first test location, while the maximum shift occurred where the core was closest and thickest $(0.30 \pm 0.01\%)$ at the third location, cf. Figure 8.

Although the larger core size at the right edge caused the strongest inductance shift, it also reduced the deformability of the lattice and limited the mobility of the core at that position.

5.3 Size + Offset

In this configuration, we combined variation in core size with lateral offset. The smallest core, with a cross-section of 25 mm^2, was placed at the leftmost edge of the coil (offset of -20 mm). The medium-sized core, with a cross-section of 100 mm^2, was positioned along the central axis (0 mm offset), while the largest core, with a cross-section of 150 mm^2, was placed at the rightmost edge (offset of 20 mm).

We evaluated the response by applying a pointed load at three locations along the lattice. When we applied force at the leftmost region, the small, off-center core was displaced but contributed little to the inductance shift $(0.01 \pm 0.002\%)$. In contrast, the medium core at the center produced a shift of $(0.04 \pm 0.003\%)$, and the largest core generated the maximum change in inductance $(0.09 \pm 0.01\%)$ when we pressed directly above it at the rightmost location (cf. Figure 8).

5.4 Distribution + Offset

In this setup, we used an asymmetrically shaped core resembling a Σ-profile, which caused non-uniform deformation under localized compression. The inter-core separation was about 28 mm at a 16 mm offset toward the left edge of the substrate, gradually reduced to 16 mm at the center, and then increased again to 28 mm at the rightmost edge.

We evaluated the response by applying force at different points on the substrate surface, which displaced varying amounts of core material into the sensing region directly above the coil. Compression at the central region led to a stronger accumulation of core elements near the coil and thus the highest inductance change $(0.31 \pm 0.01\%)$ at the central location. In contrast, compressing the rightmost area resulted in fewer cores clustering over the coil, producing a lower shift $(0.18 \pm 0.01\%)$, while pressing at the leftmost edge yielded an intermediate response $(0.22 \pm 0.01\%)$, cf. Figure 8.

5.5 Size + Distribution + Offset

In this configuration, we arranged the cores so that the left edge contained larger cores (150 mm^2 cross-section) with smaller spacing of 8 mm, while toward the right edge (offset of 20 mm) the cores became smaller (25 mm^2 cross-section) and the spacing increased to 16 mm.

We evaluated the response by applying a pointed load at three locations along the lattice. The inductance shift was highest on the left side $(0.28 \pm 0.01\%)$ at the first location, lower in the center $(0.19 \pm 0.01\%)$, and smallest on the right $(0.12 \pm 0.01\%)$. This pattern occurred because, when we compressed the left side, the larger cores combined into a greater effective core mass, whereas on the right, the smaller cores moved closer together but contributed less ferromagnetic volume within the coil's magnetic field.

As a result, the larger cores on the left made that region stiffer, while the right side remained softer due to the more flexible lattice material. This configuration therefore created a stiffness gradient across the lattice, leading to varying sensitivities along its width, cf. Figure 8.

6 Design Recommendations

Based on the experiments, we can derive several design recommendations that should be taken into account during implementation.

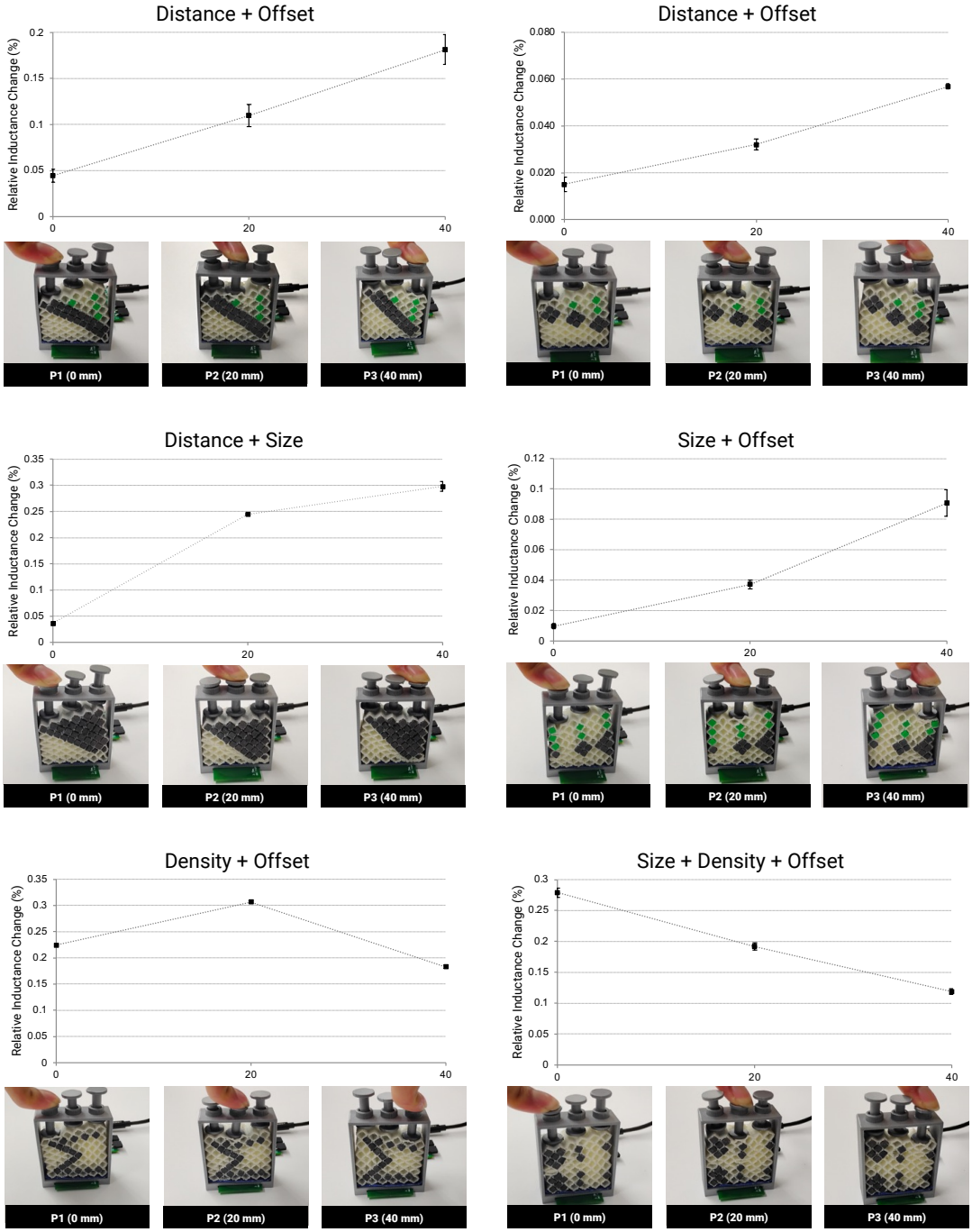

Figure 8: Samples with six different ferromagnetic core arrangements, combining multiple design parameters, are showcased in various deformed states. The corresponding graphs for 6 samples—comprising 6 different configurations of Distance + Offset (single-piece core), Distance + Offset (multiple-piece core), Distance + Size, Size + Offset, Density + Offset, and Size + Density + Offset—illustrate the relative change in coil inductance as the lattice is pressed locally at three regions: top-left (Point 1), top-center (Point 2), and top-right (Point 3). Each of these points lie at the distances of 0 mm, 20 m and 40 mm from the top-left corner of the coil.

6.1 Balancing core position for sensitivity and deformation

Our experiments show that the strongest inductance change occurs when the core is placed very close to the coil. To capture meaningful variations, the core also needs enough space to move when external forces are applied on the sensor. If the core is positioned farther away (at a distance comparable to or greater than the coil diameter), it allows larger deformations and more travel, but the inductance change becomes less pronounced for the same displacement or for small forces.

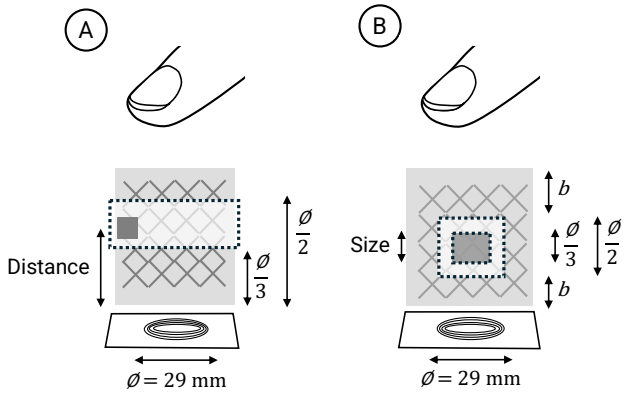

Figure 9: Recommended positioning of the core from the coil plane for higher sensitivity (A); Recommended size of the core with surrounding substrate buffer (B).

We therefore recommend positioning the core at a height between one-third and one-half of the coil diameter (i.e., $\varnothing/3$ to $\varnothing/2$, with $\varnothing \approx 29$ mm in our case, cf. Figure 9, A). This configuration provides a practical balance: the core can travel sufficiently while the sensor still achieves robust sensitivity, as shown by a relative inductance change greater than 0.39% for a displacement of 10 mm.

Summarizing, we would recommend to place the core close to the coil for maximum sensitivity, but to keep it within one-third to one-half of the coil diameter to ensure both sensitivity and deformation capacity.

6.2 Core geometry: trading off size, sensitivity, and flexibility

We found that increasing the core size enhanced the relative change in inductance. For example, a core edge length between one-third and one-half of the coil diameter ($\varnothing/3$ to $\varnothing/2$) already provides a measurable benefit, with observed inductance changes exceeding 0.15% for a 10 mm displacement, cf. Figure 9, B. Of course, larger cores provide a higher sensitivity. However, the drawback of a larger solid mass embedded in the lattice is reduced structural flexibility, which can make the sensor stiffer. To counteract this effect, sufficient lattice padding should be used around the core so that it still has room to travel towards the coil.

In practice, if the sensing goal is to capture smaller displacements with high precision, smaller cores closer to the coil are more effective. Conversely, if larger deformations must be measured (beyond about half the coil diameter), larger cores placed slightly farther from the coil can be used, provided that the substrate allows enough travel and maintains a soft interface for comfortable user interaction.

Summarizing, we notice that larger cores increase sensitivity but reduce flexibility. Therefore, we recommend to use smaller cores close to the coil for precise sensing, and larger cores farther away when targeting larger deformation ranges.

6.3 Core configuration: using asymmetry for variable sensitivity

An asymmetric placement of the cores within the lattice, for example, by introducing lateral offsets greater than half the coil diameter ($o > \varnothing/2$), can produce variable inductance responses. This effect can be deliberately exploited to define multiple interaction regions along the sensor interface, enabling richer and more diverse input possibilities. Extending this idea, multiple cores with different heights above the coil plane or with varying lateral offsets can be combined to create sensors that respond differently across distinct regions.

We also observe that using multiple smaller cores in an asymmetric configuration can outperform a single large core. With discretized cores, the substrate can deform locally, allowing forces applied at different zones to be captured independently. In contrast, a single large core tends to enforce more uniform deformation, which reduces the differential sensitivity of the sensor.

To enable multi-dimensional sensing with only one coil, we should place the cores asymmetrically ($o > \varnothing/2$) and consider using multiple smaller cores instead of a single large one. This approach enhances localized deformability and allows for variably sensitive interactive surfaces, such as pressure-based sliders, with only one readout coil.

6.4 Core configuration in relation to sensor dimensions

When the available sensor "footprint" is limited, the choice of core size and distribution becomes a key factor in achieving strong inductance variations. Larger cores positioned close to the coil, combined with a stable substrate, are well suited for detecting very small displacements or tilts of the core, since even minor movements produce measurable inductance shifts. In contrast, smaller cores provide a greater range of motion and are therefore useful when the sensor is intended to capture larger deformations across a wider area.

Distributed core arrangements are particularly effective for sensing under large-scale deformations of the lattice, because they can respond to stronger forces applied across the body of the material. Conversely, concentrated core configurations work better for localized sensing tasks, where even small core displacements need to be reliably detected.

Summarizing, we can say that for compact sensors, we recommend to use larger cores close to the coil to maximize sensitivity to small displacements. For larger-area sensors or applications requiring greater deformation range, distribute smaller cores across the substrate to ensure robust responses to high-magnitude forces.

6.5 Core configuration for tailored deformation behavior

In some cases, the arrangement of the core material not only determines the inductive response but also directly influences how the lattice deforms under applied pressure. A large single-piece core (especially when its size exceeds twice the coil diameter) was found to increase rigidity, thereby stiffening the lattice. In contrast, heterogeneous configurations with variable core sizes create regions of different compressibility within the same lattice. This enables deformation patterns in which the structure can pivot around a point anchored by a larger core volume, redistributing forces in a non-uniform way.

Summarizing, we can combine rigid and flexible core elements within the same structure to design custom deformation behavior and enable richer interaction modes such as tilt or pivot, in addition to conventional compression.

6.6 Lattice design for deformability and sensitivity

The geometric characteristics of the lattice (type, cell size, and wall thickness) certainly plays an important role in determining both deformability and sensing performance. Softer lattices (e.g., realized through larger cell sizes, thinner walls) allow the geometry to deform more effectively under pressure. This in turn enhances deformation tracking and increases the displacement of the embedded ferromagnetic cores.

In our experiments, the square-grid lattices achieved strain values between 25% and 33% under compression. Examples include 4.2 mm unit cell size with 0.8 mm wall thickness ($s/t = 5.25$, using the 85A TPU), 4.4 mm unit cell size with 0.4 mm wall thickness ($s/t = 11$, using 95A TPU), or finer structures such as 2 mm unit cell size with 0.2 mm wall thickness ($s/t = 10$, using 95A TPU). BCC lattices with 6 mm unit cell size and 1 mm beam thickness ($s/t = 6$, 95A TPU) also demonstrated high compressibility. Furthermore, modified square-grid cells with 8 mm unit cell size and 0.4 mm wall thickness ($s/t = 20$, 95A TPU) were designed with serpentine walls to increase stretchability, achieving up to 39% strain.

Greater deformability (whether from compression or elongation) leads to larger core displacements and therefore stronger inductance shifts. At the same time, softer and more compliant substrates provide a comfortable interface for human interaction.

Summarizing, we recommend to use lattice structures to tune the balance between sensitivity and rigidity. Larger cells and thinner walls increase deformability and sensitivity, while stretchable lattice designs (e.g., serpentine walls) enable multidimensional deformation. Therefore, designers should select lattice parameters according to the deformation they wish to sense—compression, elongation, or stretch—and integrate cores accordingly.

Through these explorations, we demonstrate how users can modify ferromagnetic core arrangements to tune the sensing characteristics of the structure according to specific needs. Our study thus provides a framework for custom-designing pressure-sensitive substrates—offering users a way to define the sensor's spatial sensitivity profile and mechanical behavior through core placement and distribution strategies.

7 Evaluating Sensor Performance

In order to evaluate the performance of our sensor, we calculated its sensitivity and examined its long-term stability in terms of inductance change over 10,000 cycles of compression and decompression, using one sensor sample with a uniform core layer positioned 15 mm above the readout coil. We utilized an automated compression testing setup based on a 3-axis CNC mill, equipped with a movable actuator head, to systematically compress the sensor's top surface by controlled distances or for specified time intervals for the evaluation.

7.1 Sensitivity

In our case, sensitivity refers to the measure of how much the inductance changes when there is a minute compression in the sensor's lattice structure, which in turn causes a change in the core position relative to the readout coil. Hence, we compressed the sensor top in small incremental steps of 0.2 mm, till 10 mm, which also displaced the core in the same way, and paused for 30 seconds at each step to record the inductance reading at a particular step. We selected the step size and dwell time to keep the experiment duration manageable while capturing high-resolution inductance data, since the sensitivity evaluation was based on the average relative inductance values from three loading and unloading cycles. However, since the inductance values saturated beyond 6 mm for our chosen sample, we present data only within the 0 – 6 mm displacement range. We observe that our sensor achieves a sensitivity of up to 0.233% change in relative inductance per millimeter of compression, as estimated from the slope of a linear fit of inductance values within the 0 – 2 mm compression range (cf. Figure 10). We emphasize that the calculated sensitivity values is specific to the tested sensor variant, and may vary across other core–lattice configurations. This variant was selected to evaluate the sensing performance under small, touch-scale deformations.

7.2 Stability

To evaluate long-term performance or the stability of our sensor, we use the same test setup and compress and decompress our sensor sample by 10 mm for 10,000 cycles, and record the inductance over time. We inspect the shift in the maximum inductance value over time as our sensor undergoes repetitive deformation and find that our sensor remains very stable, as the difference between the peak inductance values (when the sensors are compressed beyond 6 mm) between the 1st and 10,000th cycle remains within 0.05% of the initial inductance values (cf. Figure 10). Hence, we observe only minimal drift in the inductive response of our sensor sample even after prolonged use over 10,000 cycles, which eliminates the need for frequent sensor recalibration during regular operation.

The observed drift over the test duration can be attributed to the viscoelastic behavior of TPU, possible minor plastic deformation under repeated loading, and material inhomogeneities introduced during the FDM fabrication of the TPU lattice. Although these drifts can be further reduced through optional sensor calibration at the beginning of extended or distinct usage sessions, machine learning–based compensation approaches could be explored as part of future work that account for cycle-dependent material deformation effects across repeated loading cycles.

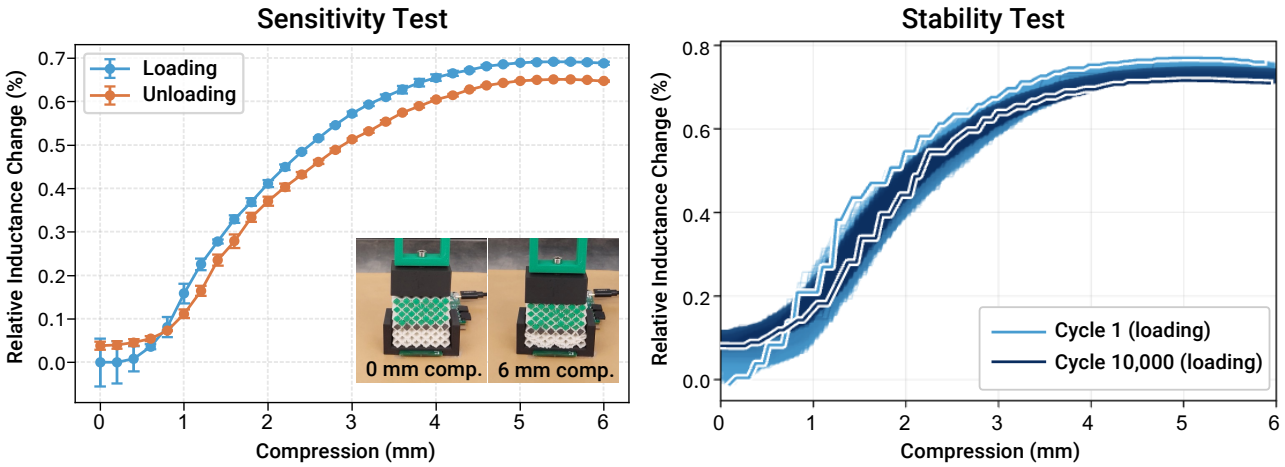

Figure 10: Calculating the sensitivity of our sensing approach: We measure the relative inductance change under incremental compression using an automated compression setup and compute sensitivity as the slope of a linear fit between 0 to 2 mm compression of the sensor (left). Evaluating long-term stability: We track the relative inductance change over 10,000 loading cycles and evaluate drift by comparing the maximum inductance values between the initial and final loading cycles (right).

8 Applications: Real World Use-Case Scenarios

In this section, as well as in the accompanying video, we demonstrate different demo applications, including a highly sensitive liquid volume measurement, an interactive on-surface music controller, a highly stretchable hand-held controller, and a highly precise smart shoe sole - employing variations in the geometric and spatial arrangement of the core and lattice, together with the use of single or multiple coils. In all these applications, a calibration step was performed at the beginning, where the minimum and maximum values were detected and subsequently used to linearly map the sensing data.

8.1 Liquid Level Measurement

Firstly, we show a soft lattice structure with embedded ferromagnetic components, designed to support everyday liquid bottle enabling real-time measurement of the liquid volume inside it. The lattice–core structure rests on a casing that houses the coil, which is fixed on a tabletop surface, cf. Figure 11. The sensing principle is based on the deformation of the lattice under the bottle's weight, which displaces the embedded core particles and alters the coil's inductance.

For this implementation, we used a soft yet stable lattice with a unit cell size of 6 mm and a beam thickness of 1 mm, a configuration that provided high deformation and, consequently, substantial core displacement. A similar lattice parameter configuration has also been reported to provide the highest comparative sensitivity (−0.17% kPa^{-1}) in related work [3]. The core layer is embedded 12 mm above the coil plane (approximately one-third of the coil diameter), which increased the application's sensitivity to small variations in bottle weight and allows detection of subtle changes in liquid volume. To ensure uniform response, we arranged the ferromagnetic cores

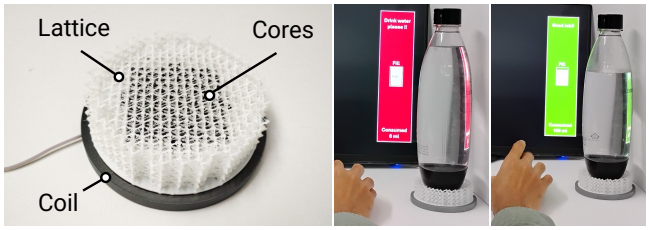

Figure 11: Real-world use case scenarios of our sensing approach: a smart pressure-sensitive structure for measuring liquid volume or weight. The structure having 60 mm diameter in size and 24 mm height comprises of BCC lattice structure with embedded ferromagnetic particles at a distance of 12 mm from the base, housing the coil (left); Demonstration of the pressure sensitive structure in action with the visualization of the amount of liquid stored in the bottle placed on the sensor, based on the sensor output. When the bottle is full, the interface alerts the user to drink water (based on the bottle weight onto the sensor); the user gets prompted to drink water and upon detecting the weight change in the liquid, the user gets a congratulatory notification, stating the amount of water consumed (right).

symmetrically about the central axis, ensuring even distribution across the coil's active area.

Accurate estimation of liquid volume is achieved through an initial calibration step: we recorded the inductance shift with the empty bottle and then when fully filled. Intermediate inductance values are linearly mapped to the corresponding liquid volume, enabling real-time visualization of the water level. All sensor data was streamed from the MSP430 microcontroller to an open-source

graphical rendering environment, producing a dynamic display of the estimated volume, cf. Figure 11.

8.2 On-surface Music Controller

We next demonstrate a compact on-surface music controller that is based on a ferromagnetic core shaped as a solid triangular prism embedded in a TPU lattice with dimensions of approximately 4 cm × 2 cm × 2 cm. We then place the controller on top of a coil base fixed to a surface, where it functions as a custom input device. By using the prism geometry, we enable manipulation of the controller through forward and backward pivoting, cf. Figure 12.

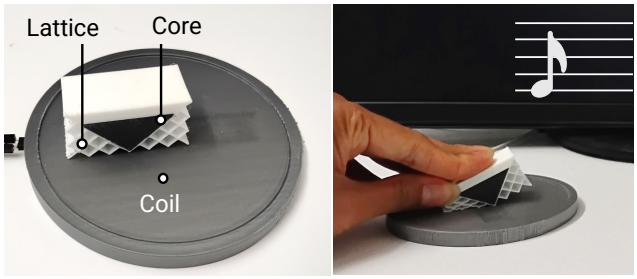

Figure 12: A pressure-sensitive controller with the core shaped as a triangular prism (left); demonstration of the tangible as a music controller, where tilting forward or backward allows playing music by selecting notes from an ordered arrangement (right).

To maximize responsiveness, the core is positioned just beyond the coil's edge, with its central axis offset from the coil's axis by approximately one coil radius. As the core pivots, the effective ferromagnetic volume interacting with the coil's magnetic field varies due to the combined influence of its geometry and the shifting location of its center of mass relative to the coil. When tilted toward the coil, inductive coupling increases, reaching its maximum response. In the upright neutral position, the inductance returns to baseline, while tilting away from the coil reduces coupling, dropping the inductance below baseline. This configuration thus produces a continuous range of inductance shifts around a baseline value, which can be mapped to application-specific functions. In our prototype, we directly map the inductance range to the selection of musical notes arranged by increasing frequency, enabling a simple, tangible music composition interface.

8.3 Squeezer and Game-Controller

We next demonstrate two stretchable controllers: one with a single coil and another with two coils. In the first, we built a stretchable lattice with embedded ferromagnetic cores that could be stretched and compressed uniaxially in a single-coil setup. In the second, we use the same stretchable lattice geometry with two coils to enable both in-plane compression and stretchability.

To realize these hand-held controllers, we designed modified lattice structures with wavy microstructures of varying curvature [5], which show stress–strain characteristics similar to pig belly skin. We fabricated the lattice with a cell size of 8 mm and a wall

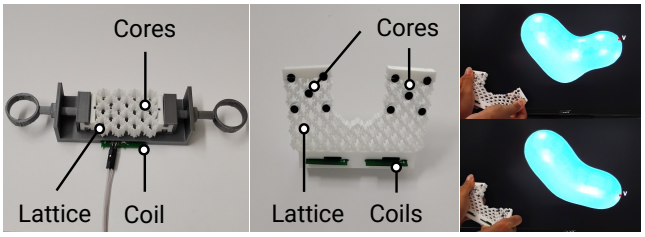

Figure 13: An uni-axial stretchable structure with stretchable cell-walls and ferromagnetic elements at the cell vertices, which we utilized for simple, planar manipulation of graphics, e.g., shrink or grow (left). We further designed a flexible hand-held controller that can deform in different directions, utilizing 2 readout coils (middle). We demonstrate a sculpting application (right).

thickness of 0.4 mm. For the uniaxial single-coil version, we embedded ferromagnetic cores of 2 mm diameter at the lattice nodes, aligned with the substrate thickness of 1.5 mm, cf. Figure 13. Once stretched, the distance between cores increased, which reduced the inductance of the coil placed underneath. When the force was released, the lattice returned to its mean position. Under compression, the cores again moved closer together, which increased the inductance. Finally, we used this controller to deform a 3D rendering accordingly in one dimension.

In a second version, we built a more advanced controller using two handles in combination with two coils and the same lattice. The handles held ferromagnetic cores of 5 mm diameter and 10 mm thickness at the lattice nodes. In this setup, the cores squeezed toward one coil while stretching away from the other, which created richer input through localized stretching and compression, cf. Figure 13.

8.4 Pressure-Sensitive Shoe Sole

Finally, we implemented a smart shoe sole that used a TPU-based lattice integrated with ferromagnetic cores for inductive pressure sensing. We used a stiffer lattice with a unit cell size of 10 mm and a beam thickness of 1.6 mm, 3D-printed in TPU so it could reliably deform under the weight of an average adult. We further embedded 6 mm ferromagnetic cores inside the lattice pockets, about 20 mm above the coil layer. The coil layer was placed directly above the lattice and beneath the shoe covering, see Figure 14.

In this prototype, we used four coils in total to detect the pressure at the front and rear of the foot and to estimate the foot's tilt along its longitudinal axis. As the user walked or shifted posture, the shoe sole lattice deformed, which displaced the embedded ferromagnetic cores and shifted the inductance measured by the four coils. The sensor data was then sent from the microcontroller to an iPhone app using OSC.

9 Discussion and Limitations

Broad Sensing Capabilities Across Interaction Types. In InSense3D, we enable a broad sensing spectrum, ranging from passive, static

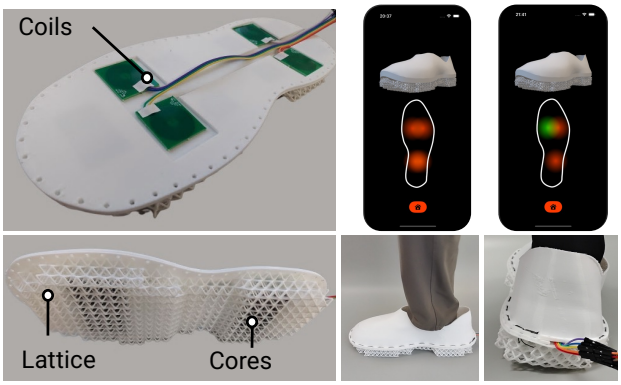

Figure 14: A shoe sole comprising a BCC lattice integrated with ferromagnetic core particles and 4 coils (left). We show a pressure heat-map visualization of the user's foot based on the inductance data recorded from the sensor (right).

load measurement to highly dynamic, stretch–squeeze gestures facilitated through our deformable controller examples. For instance, our lattice–core configurations can detect steady weights and slow temporal changes (as in liquid-level measurement), capture region-wise dynamic pressure variations such as those observed in a shoe sole during gait, and accommodate large internal deformations for active gestures (as demonstrated in our controller interfaces), while also offering soft, compliant interaction experiences. The custom-printed core shape and its placement within the lattice, alongside the lattice structure, collectively determine the region-specific deformability of the sensor, wherein each lattice-core variant enables distinct interaction characteristics. For instance, our music controller can pivot forward and backward like a toggle, while other controller structures also support push–pull and multi-axis stretching, as demonstrated in our prototypes. This freedom of interaction based on the custom lattice-core configuration is a unique characteristic of our approach, in contrast to other systems like eFlesh [21] that are primarily designed for the detection of objects in contact.

Sensitivity and Durability Put in Context. We observe that the high sensitivity values ($0.233\%\,\mathrm{mm}^{-1}$) exhibited by our sensors in the low-strain regime are beneficial for applications involving low-magnitude forces or slight force variations, such as detecting subtle changes in the volume of water consumed from a bottle (as also demonstrated in the section 8), where minimal lattice deformation or core displacement needs to be detected. The sensitivity of our sensor is comparable to printed resistive techniques such as LattiSense [24], which exhibits an overall relative-resistance change of roughly $0.01 - 0.03$ times its initial resistance, per millimeter of deformation and is capable of detecting sub-millimeter deformations. Our performance is likewise comparable to magnetic tactile approaches such as eFlesh [21], which can detect forces in the range as low as $0.2 - 0.3$ N. However, one of the key distinctions of our approach is that even after 10,000 loading–unloading cycles, our sensors remained fully functional and preserved their original dimensions, unlike LattiSense [24], which reports lattice shrinkage after repeated use. Additionally, our sensor fabrication is independent of the connectors and coil interfacing with the readout electronics, unlike other approaches [24], where connector placement determines the design of the sensitive regions of the 3D-printed lattice structures.

Coil–Lattice Placement and Design. Despite the versatility of creating an inductive-based custom deformation sensor, InSense3D has certain limitations. For instance, in the current prototypes, all sensor structures were fabricated with a planar base so that they could be mounted directly over the flat coil housing base. Though this configuration ensures consistent alignment between the ferromagnetic inserts within the lattice and the readout coil, it limits the exploration of non-planar geometries, primarily due to the inherent planarity of the coil used. However, our approach can still support deformation and interaction over curved surfaces, provided that the readout coils, which are sensing the core displacement, are mounted onto such rigid curved surfaces. Alternatively, integration with flexible coils would be an interesting future research direction to embrace fully free-form 3D interfaces.

One limitation of our InSense3D fabrication approach is that the lattice containing the ferromagnetic core inserts must remain fixed relative to the readout coil. Hence, we use PLA- or TPU-based housings to rigidly maintain the spatial configuration between the coil and the lattice. This is done since our sensor is intended for interactions that induce core displacement solely through lattice deformation, and not through changes in the lattice's overall position or any mid-air interactions. Although a key characteristic of our approach is lattice swappability over the readout coil, in some examples, such as the shoe sole and game controller, we embedded the coil within the artifact to spatially constrain the lattice. These designs, however, can be further optimized by placing the coil in a modular housing that interfaces with the TPU components to ensure easy assembly and disassembly. Additionally, the core–coil separation is another important factor in ensuring effective inductive coupling and the sensor response. For instance, we observe that for the planar coil with a diameter of 29 mm, the inductive signal begins to decrease noticeably as the core–coil separation approaches the coil diameter, while at a separation of approximately 45 mm (i.e., 1.5 times the coil diameter), the change in inductance becomes effectively negligible. This behavior is consistent with standard electromagnetic models, in which the magnetic field strength B depends on the coil radius a and the core–coil separation z, and can be approximated as $B(z) \propto (a^2 + z^2)^{-3/2}$, leading to a rapid reduction in inductive coupling at larger distances [11].

Another characteristic of the InSense3D approach is that each readout coil is configured to reliably sense a single lattice structure at a time. This is because, when multiple sensor modules with embedded ferromagnetic parts are placed within the same coil's sensing region, they collectively influence the magnetic field, resulting in combined inductive responses. Additionally, inductive responses from separate sensor modules that are symmetrically arranged about the same coil axis cannot be individually distinguished, thereby indicating certain sensing limitations when using a single coil.

Regarding the size constraints, the smallest practical configuration requires at least two layers: one enabling core displacement and another housing the inserts. This yields a 2×2 extruded square-grid

lattice or a 2×2×2 BCC unit-cell arrangement that preserves fabrication feasibility and structural stability. However, the lattice design should be based on the apt use-case requirements with sufficient internal space for core displacement.

Robustness to Environmental Interference. To minimize interference from external ferromagnetic objects near our sensor, we design the system such that the lattice fully covers the surface area of the coil and acts as a barrier between the coil and the surroundings, which ensures that the embedded ferromagnetic inserts are the only components influencing the coil's magnetic field for deformation sensing. We did not encounter any noticeable interference effects or noise in our readings, as the lattice structure surrounded the coil completely, with the overall lattice height generally exceeding the coil diameter, which prevents nearby objects or even a user's fingers, from influencing the coil's magnetic field. However, we strongly discourage bringing magnets or moving solid ferromagnetic metal parts close to the sensor, as such conditions can alter the magnetic field.

10 Conclusion and Future Work

In this work, we introduced *InSense3D*, a design and fabrication approach that embeds 3D-printed ferromagnetic cores into deformable TPU lattice to enable wire-free inductive sensing. By systematically studying the design parameters — core–coil distance, lateral offset, size, and density — we showed how geometric and spatial configurations directly influence sensitivity, responsiveness, and deformation behavior. Extending beyond single-parameter explorations, we demonstrated multi-parameter core arrangements that yield richer sensing characteristics and asymmetric responses, offering designers a means to customize inductive behavior at both local and global scales.

Through four application examples we highlighted the versatility of our approach. Across these scenarios, we enable the creation of passive and high-fidelity sensing interfaces that require neither embedded electronics nor wiring, lowering barriers for iterative prototyping and tangible interaction design.

While our study focuses on geometric configurations and their influence on inductive coupling, for future work we should extend to material-level variations, such as co-printing with filaments of varying stiffness to further tune sensitivity and mechanical performance. Though we addressed the stiffening of the core caused by large core inserts by utilizing distributed, multiple smaller cores, future work could explore developing and using TPU filaments infused with ferromagnetic particles. Moreover, scaling this approach toward higher-resolution sensing, e.g., by embedding arrays of distributed cores and pairing them with multi-coil readout systems, could enable more detailed deformation mapping across a wide range of interfaces. As part of future work, we are also developing a design and analysis tool that can automatically generate the 3D geometries of lattice–core configurations based on user-defined requirements such as desired sensitivity (i.e., uniform or variable, or along single-axis or multi-axis), lattice geometry, bounding volume, or input shape. The tool will further evaluate how each generated structure influences the coil's magnetic field, enabling informed design choices early in the workflow. Moreover, algorithms can also be developed to recognize different lattice configurations on a single-coil platform by analyzing shifts in baseline inductance, enabling automatic detection when lattices are swapped or when new lattice modules are introduced, as per the use-case scenario, to fully implement plug-and-play sensing with simplified calibration.

Acknowledgments

This work is supported in part by the European Union – Next-Generation EU (Piano Nazionale di Ripresa e Resilienza (PNRR) — Missione 4, Componente 2, Investimento 3.3 — Decreto del Ministero dell'Università e della Ricerca n. 352 of April 9, 2022). This work is also partially funded by the Autonomous Province of Bozen-Bolzano through the South Tyrol European Regional Development Fund (ERDF/FESR) Programme under Projects EFRE/FESR 1011 (SmartCover) and EFRE/FESR 1007 (iPlayground). The work is further supported in part by the National Science Foundation under Award No. IIS-2443190. We also express our thanks to Andreas Pointner (Free University of Bozen-Bolzano) for assistance with video editing and compilation of the accompanying video submission.

References

[1] Marwa AlAlawi, Regina Zheng, Sooyeon Ahn, Katherine Yan, Ticha Sethapakdi, Junyi Zhu, and Stefanie Mueller. 2025. Meta-antenna: Mechanically Frequency Reconfigurable Metamaterial Antennas. In *Proceedings of the 38th Annual ACM Symposium on User Interface Software and Technology*. ACM, Busan Republic of Korea, 1–19. doi:10.1145/3746059.3747760

[2] Kalman Babkovic, Milica Kisic, and Mirjana Damnjanovic. 2023. 3-D Printed Inductive Displacement/Force Sensor. *IEEE Trans. Magn.* 59, 2 (Feb. 2023), 1–5. doi:10.1109/TMAG.2022.3218025

[3] Rahul Bhaumik, Thomas Preindl, Alexandra Ion, Camilo Ayala-Garcia, Nitzan Cohen, Michael Haller, and Niko Münzenrieder. 2025. Inductive Pressure Sensors Using 3D-Printed Structures With Tunable Stiffness. *IEEE Sensors Letters* 9, 5 (May 2025), 1–4. doi:10.1109/lsens.2025.3562455

[4] Sergio De La Rosa, Pedro F. Mayuet Ares, and Lucía Rodríguez-Parada. 2025. Design of Flexible TPU-Based Lattice Structures for 3D Printing: A Comparative Analysis of Open-Cell Versus Closed-Cell Topologies. *Polymers* 17, 9 (April 2025), 1133. doi:10.3390/polym17091133

[5] Le Dong, Dong Wang, Jinqiang Wang, Chengru Jiang, Hui Wang, Biao Zhang, Mao See Wu, and Guoying Gu. 2022. Modeling and Design of Periodic Polygonal Lattices Constructed from Microstructures with Varying Curvatures. *Physical Review Applied* 17, 4 (April 2022), 044032. doi:10.1103/PhysRevApplied.17.044032

[6] Winncy Y. Du. 2014. *Resistive, Capacitive, Inductive, and Magnetic Sensor Technologies* (0 ed.). CRC Press. doi:10.1201/b17685

[7] Charles El Helou, Philip R. Buskohl, Christopher E. Tabor, and Ryan L. Harne. 2021. Digital logic gates in soft, conductive mechanical metamaterials. *Nature Communications* 12, 1 (March 2021), 1633. doi:10.1038/s41467-021-21920-y

[8] Jun Gong, Olivia Seow, Cedric Honnet, Jack Forman, and Stefanie Mueller. 2021. MetaSense: Integrating Sensing Capabilities into Mechanical Metamaterial. In *The 34th Annual ACM Symposium on User Interface Software and Technology*. ACM, Virtual Event USA, 1063–1073. doi:10.1145/3472749.3474806

[9] Jun Gong, Yu Wu, Lei Yan, Teddy Seyed, and Xing-Dong Yang. 2019. Tessutivo: Contextual Interactions on Interactive Fabrics with Inductive Sensing. In *Proceedings of the 32nd Annual ACM Symposium on User Interface Software and Technology (UIST '19)*. Association for Computing Machinery, New York, NY, USA, 29–41. doi:10.1145/3332165.3347897

[10] Serena Graziosi, Federico Maria Ballo, Flavia Libonati, and Sofia Senna. 2022. 3D printing of bending-dominated soft lattices: numerical and experimental assessment. *Rapid Prototyping Journal* 28, 11 (May 2022), 51–64. doi:10.1108/RPJ-03-2022-0095

[11] David J. Griffiths. 2023. *Introduction to Electrodynamics* (5 ed.). Cambridge University Press. doi:10.1017/9781009397735

[12] Alexandra Ion, Johannes Frohnhofen, Ludwig Wall, Robert Kovacs, Mirela Alistar, Jack Lindsay, Pedro Lopes, Hsiang-Ting Chen, and Patrick Baudisch. 2016. Metamaterial Mechanisms. In *Proceedings of the 29th Annual Symposium on User Interface Software and Technology*. ACM, Tokyo Japan, 529–539. doi:10.1145/2984511.2984540

[13] Alexandra Ion, David Lindlbauer, Philipp Herholz, Marc Alexa, and Patrick Baudisch. 2019. Understanding Metamaterial Mechanisms. In *Proceedings of the 2019 CHI Conference on Human Factors in Computing Systems*. ACM, Glasgow Scotland Uk, 1–14. doi:10.1145/3290605.3300877

[14] Nimal Jagadeesh Kumar, Alexander Johnson, Robert Cobden, George Valsamakis, J.Gene Gristock, Arash Pouryazdan, Daniel Roggen, and Niko Münzenrieder. 2023. A Flexible Inductive Sensor for Non-Invasive Arterial Pulse Measurement. In *2023 IEEE SENSORS*. IEEE, Vienna, Austria, 1–4. doi:10.1109/sensors56945.2023.10324884

[15] Hsuanling Lee and Liang He. 2024. 3D Printing Shape-Changing Devices with Inductive Sensing. In *ACM SIGGRAPH 2024 Posters (SIGGRAPH '24)*. Association for Computing Machinery, New York, NY, USA, 1–2. doi:10.1145/3641234.3671039

[16] Hsuanling Lee, Yujie Shan, Huachao Mao, and Liang He. 2024. Fluxable: A Tool for Making 3D Printable Sensors and Actuators. In *The 37th Annual ACM Symposium on User Interface Software and Technology*. ACM, Pittsburgh PA USA, 1–3. doi:10.1145/3672539.3686342

[17] Hanchuan Li, Eric Brockmeyer, Elizabeth J. Carter, Josh Fromm, Scott E. Hudson, Shwetak N. Patel, and Alanson Sample. 2016. PaperID: A Technique for Drawing Functional Battery-Free Wireless Interfaces on Paper. In *Proceedings of the 2016 CHI Conference on Human Factors in Computing Systems (CHI '16)*. Association for Computing Machinery, New York, NY, USA, 5885–5896. doi:10.1145/2858036.2858249

[18] Mingming Li, Jiaji Li, Haotian Chen, Dingning Cao, Karla Sahin, and Stefanie Mueller. 2025. Integrating Motion Sensing into 3D-Printed Bending Structures. In *Adjunct Proceedings of the 38th Annual ACM Symposium on User Interface Software and Technology*. ACM, Busan Republic of Korea, 1–3. doi:10.1145/3746058.3758350

[19] Doga Ozbek, Marwa AlAlawi, and Michael Wessely. 2025. AcceloPrint: Fabricating Customizable Accelerometers with Multi-Material 3D Printing. In *Proceedings of the Extended Abstracts of the CHI Conference on Human Factors in Computing Systems*. ACM, Yokohama Japan, 1–8. doi:10.1145/3706599.3720059

[20] Oliver Ozioko, Marion Hersh, and Ravinder Dahiya. 2019. Inductance-Based Soft and Flexible Pressure Sensors using Various Compositions of Iron Particles. In *2019 IEEE SENSORS*. IEEE, Montreal, QC, Canada, 1–4. doi:10.1109/sensors43011.2019.8956646

[21] Venkatesh Pattabiraman, Zizhou Huang, Daniele Panozzo, Denis Zorin, Lerrel Pinto, and Raunaq Bhirangi. 2025. eFlesh: Highly customizable Magnetic Touch Sensing using Cut-Cell Microstructures. doi:10.48550/ARXIV.2506.09994

[22] Thomas Preindl, Andreas Pointner, Nimal Jagadeesh Kumar, Nitzan Cohen, Niko Münzenrieder, and Michael Haller. 2025. SqueezeMe: Creating Soft Inductive Pressure Sensors with Ferromagnetic Elastomers. In *Proceedings of the 2025 CHI Conference on Human Factors in Computing Systems*. ACM, Yokohama Japan, 1–13. doi:10.1145/3706598.3713369

[23] Huilin Ren, Xiaodan Yang, Zhenhu Wang, Xuguang Xu, Rong Wang, Qi Ge, and Yi Xiong. 2022. Smart structures with embedded flexible sensors fabricated by fused deposition modeling-based multimaterial 3D printing. *IJSNM* 13, 3 (July 2022), 447–464. doi:10.1080/19475411.2022.2095454

[24] Rei Sakura, Changyo Han, Yahui Lyu, Keisuke Watanabe, Ryosuke Yamamura, and Yasuaki Kakehi. 2023. LattiSense: A 3D-Printable Resistive Deformation Sensor with Lattice Structures. In *Proceedings of the 8th ACM Symposium on Computational Fabrication (SCF '23)*. Association for Computing Machinery, New York, NY, USA. doi:10.1145/3623263.3623361

[25] Munehiko Sato, Ivan Poupyrev, and Chris Harrison. 2012. Touché: enhancing touch interaction on humans, screens, liquids, and everyday objects. In *Proceedings of the SIGCHI Conference on Human Factors in Computing Systems (CHI '12)*. Association for Computing Machinery, New York, NY, USA, 483–492. doi:10.1145/2207676.2207743

[26] Martin Schmitz, Mohammadreza Khalilbeigi, Matthias Balwierz, Roman Lissermann, Max Mühlhäuser, and Jürgen Steimle. 2015. Capricate: A Fabrication Pipeline to Design and 3D Print Capacitive Touch Sensors for Interactive Objects. In *Proceedings of the 28th Annual ACM Symposium on User Interface Software & Technology (UIST '15)*. Association for Computing Machinery, New York, NY, USA, 253–258. doi:10.1145/2807442.2807503

[27] Ryan L. Truby, Lillian Chin, Annan Zhang, and Daniela Rus. 2022. Fluidic innervation sensorizes structures from a single build material. *Science Advances* 8, 32 (Aug. 2022). doi:10.1126/sciadv.abq4385

[28] Yang Zhang, Gierad Laput, and Chris Harrison. 2017. Electrick: Low-Cost Touch Sensing Using Electric Field Tomography. In *Proceedings of the 2017 CHI Conference on Human Factors in Computing Systems (CHI '17)*. Association for Computing Machinery, New York, NY, USA, 1–14. doi:10.1145/3025453.3025842